Rock Mech. Rock Engng. (2006) 39 (4), 315–338
DOI 10.1007/s00603-005-0066-3

Rock Mechanics and Rock Engineering
Printed in Austria

A Simple Method for Analysis of Point Anchored Rockbolts in Circular Tunnels in Elastic Ground

By

A. Bobet

Purdue University, West Lafayette, Indiana, U.S.A.

Received May 27, 2004; accepted May 27, 2005
Published online August 19, 2005

Summary

A simple analytical method for the analysis of point anchored rockbolts is presented in this paper. The solution has been derived for elastic ground and rockbolts, for plane strain conditions, and for tunnels with circular cross section. The method provides accurate results for the rockbolts' loads and displacements and explicitly includes the connection of the rockbolts to the surrounding ground. The addition of such details to a Finite Element numerical model is critical; otherwise the solution obtained may be dependent on the discretization used and on the stiffness of rockbolts and ground. As an alternative to including details of the rockbolt head and anchor point in the numerical model, which could be computationally very expensive, an equivalent spring constant is proposed. The spring constant is obtained by matching numerical with analytical results for a simple case, but keeping the geometry, material properties, and discretization unchanged.

Keywords: Tunnel, point anchored rockbolts, elastic, analytical solution.

1. Introduction

A tunnel support must sustain the load induced by the ground as it is excavated. Different types of support can be used such as concrete or shotcrete liners, steel sets, ungrouted or grouted rockbolts, etc. The design of the support often requires the use of complex numerical methods that can take into account the inherently three dimensional nature of the problem, the non-linear response of the ground and the support, and the construction process (Hoek and Brown, 1982; Aristorenas, 1992; Einstein and Bobet, 1997; Bobet et al., 1998; Gioda and Swoboda, 1999; Kawamoto and Aydan, 1999; Carranza and Fairhurst, 2000; Augarde and Burd, 2001; Eberhardt, 2001; Alonso et al., 2003; Zhu et al., 2003; Kasper and Meschke, 2004; Lee and Nam, 2004; Muniz de Farias et al., 2004; Potyondy and Cundall, 2004; Shalabi, 2005). Such numerical analyses may demand a substantial effort during modeling, problem solution, and interpretation of results, and they often require multiple iterations to find the optimum design.

Simple analytical solutions have the advantage of providing with very little effort an initial estimate of the support loads. In some cases this approximation may be sufficient for design. In other cases a numerical solution will be required; however the initial estimate provided by the analytical solution can be used as a first iteration. In addition, analytical solutions include all the fundamental variables and thus they are useful to identify those factors that are the most critical, and to verify numerical methods. Such simple solutions are available in only very few cases. For example the relative stiffness method for dry ground (Einstein and Schwartz, 1979) or for saturated ground (Bobet, 2001, 2003) is applicable to tunnels with a circular liner. Empirical or semi-empirical methods (Hoek and Brown, 1982; Sinha, 1989) often rely on the subjective judgment and experience of the designer.

Rockbolts are often used as a tunnel support. Two types can be distinguished (Hoek and Brown, 1982): (1) point anchored rockbolts; and (2) full or partial length grouted rockbolts. Point anchored rockbolts are connected to the surrounding ground either mechanically or chemically (grout or resin) through a small length compared to the length of the rockbolt shaft; the rest of their length is left ungrouted. The connection to the tunnel wall is usually accomplished with a bolted head and a steel plate. Point anchored rockbolts are loaded due to the relative movements of the ground between the anchor head and the anchor point, and thus their behavior can be separated from that of the surrounding ground. Full or partial length grouted rockbolts do not behave independently of the ground and work as a ground reinforcement (Stille et al., 1989).

Full or partial length grouted rockbolts are routinely used as tunnel support and have received significant attention in the technical literature (Sharma and Pande, 1988; Stille et al., 1989; Tannant et al., 1995; Oreste and Peila, 1996; Li and Stillborg, 1999; Serrano and Olalla, 1999; Chen et al., 2004; Cai et al., 2004a, b; Grasselli, 2005). Point anchored rockbolts are not as common, but they have the advantage of providing, if needed, an initial pre-stressing to the surrounding rock. Comparatively much less effort has been dedicated to their behavior (Farmer, 1975; Hoek and Brown, 1982; Labiouse, 1996; Windsor, 1997; Bobet, 2002; Liu et al., 2005)

There are no closed-form solutions to estimate the loads in point anchored rockbolts or, for that matter, for the design of tunnels with these rockbolts. Since point anchored rockbolts work because of the extension between the anchor head and the anchor point, they are often introduced into a numerical scheme (e.g. a Finite Element Model) as springs. The springs elongate because of the relative movement of the ground between the points of connection (head and anchor), which creates a reaction from the rockbolts in the form of two identical concentrated forces of opposite direction applied at the head and at the anchor points. This is a scheme that has been used in tunnels, anchored walls, etc. The scheme is not always correct and may introduce errors, which are dependent on the mesh used and on the stiffness of the rockbolt (spring) and ground. This is illustrated with the numerical computation of the displacements between two points, where two collinear and opposite forces are applied. The two points are spaced two units and are placed in an infinite elastic medium (Fig. 1). The results have been obtained with the code ABAQUS (Hibbit et al., 2002), a Finite Element Method (FEM) program, with the assumption of plane strain and Poisson's ratio $\nu = 0.2$. Figure 1 plots the displacements as a function of the number of elements used between the two points. The figure shows that the displacements

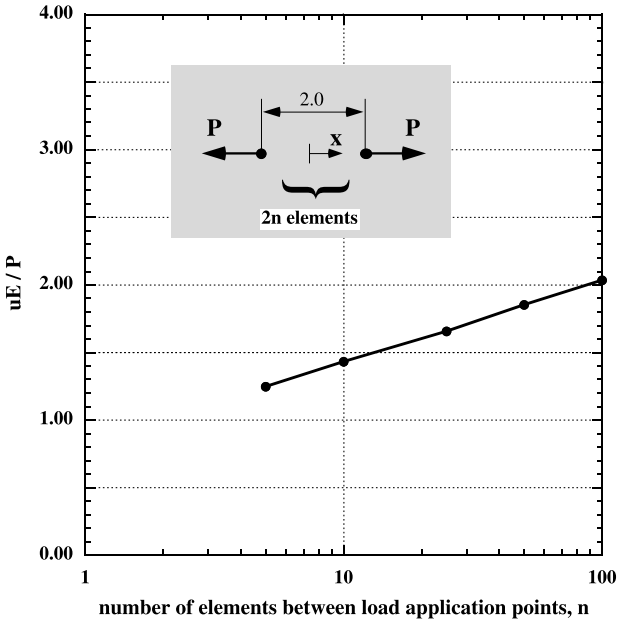

Fig. 1. Effect of discretization on displacements produced by a pair of concentrated forces in infinite medium. uE/P = normalized displacement between load application points

increase with the number of elements. The analytical solution of this problem can be found in Timoshenko and Goodier (1970) for plane stress. With the transformation of the elastic constants E (plane strain) $= E/(1-\nu^2)$, and ν (plane strain) $= \nu/(1-\nu)$, one gets for plane strain:

$$\frac{uE}{P} = -\frac{(1+\nu)(3-4\nu)}{8\pi(1-\nu)} \ln\left(\frac{1-x}{1+x}\right)^2, \tag{1}$$

where u is the horizontal displacement of a point located at a distance x from the center between the two loads (Fig. 1); E and ν are the Young's modulus and the Poisson's ratio of the medium, respectively; and P is the magnitude of the load. The displacement at the points of application of the load ($x=-1$ or $x=1$) is infinite. The results of Fig. 1 can be viewed as the rate of convergence of the FE analysis towards the exact solution. This rate is very slow, as denoted by the small increase of displacement with the number of elements, which is shown in a logarithmic scale.

Figure 2 shows the results obtained with ABAQUS of the load, P, of a rockbolt of unit length, placed on a tunnel of unit radius, in an infinite medium subjected to a uniform far field stress of unit magnitude. This is a 2D analysis where point anchored rockbolts are modeled as springs. The results are obtained for different ratios of stiffness of the medium and the rockbolt, defined by the Young's modulus of the medium, E, and the rockbolt spring constant, k (the force required to produce a unit elongation of the spring); the Poisson's ratio is always $\nu = 0.2$. The figure shows that the load is highly dependent on the discretization used, defined as the number of elements between the tunnel perimeter and the end of the rockbolt (all the elements

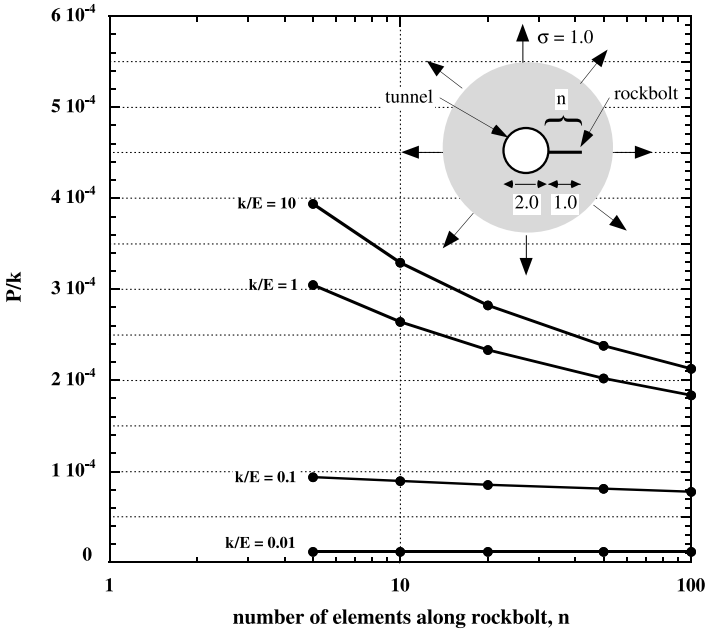

Fig. 2. Effect of discretization and stiffness on point anchored rockbolt loads. $P/k =$ Normalized load with respect to rockbolt spring constant

are approximately square). As the number of elements increases, the load of the rockbolt decreases; this is so because the displacements induced by the load increase with the number of elements (see Fig. 1). What is interesting is that the load strongly depends on the relative stiffness between the anchor and the medium. For a soft anchor (stiff medium), the solution is quite insensitive to the discretization. This is not the case for a medium relatively soft compared with the anchor; in this case the solution is very sensitive to the discretization used. Since tunnel support with rockbolts is a displacement-driven problem (the rockbolts take load because of the ground deformations) it is expected that modeling of rockbolts as springs, without consideration of how the load is transferred between the rockbolt and the ground (i.e. as a concentrated load), may result in inaccurate rockbolts' loads while the displacements obtained may be reasonable.

The paper presents a simple method for the analysis of anchored rockbolts in deep tunnels and provides recommendations, in the form of an equivalent stiffness, which can be incorporated in a numerical method. The following assumptions are made:

(i) Elastic behavior of the ground and the rockbolts.
(ii) Circular cross section of the tunnel.
(iii) Plane strain conditions on any cross section perpendicular to the tunnel axis.
(iv) Deep tunnel: the ground can be considered weightless. The errors introduced with this assumption are small for tunnels located at a depth of at least five times the tunnel radius (Bobet, 2003).

In the following discussion the geomechanics sign convention is used, with compression positive and tension negative.

2. Analytical Solution

The problem that will be solved is shown in Fig. 3. It consists of a tunnel with a circular cross section supported by rockbolts with far field stresses σ_v and σ_h (no pore pressures are considered, thus total stresses and effective stresses coincide). The following is a list of the variables used:

c	anchor head dimension
d_s	rockbolt diameter
E, ν	Young's modulus and Poisson's ratio of the ground
E_s	Young's modulus of rockbolts
k	spring constant
k_o	coefficient of earth pressure at rest; $k_o = \sigma_h/\sigma_v$
L	anchored length of rockbolt
P	rockbolt load
r, θ	polar coordinates
r_o	tunnel radius
ρ	rockbolt length measured from the center of the tunnel
S	spacing of rockbolts along tunnel axis
σ_v, σ_h	far field vertical and horizontal stresses
σ_r, σ_θ, $\tau_{r\theta}$	stresses in polar coordinates
U_r, U_θ	displacements in polar coordinates

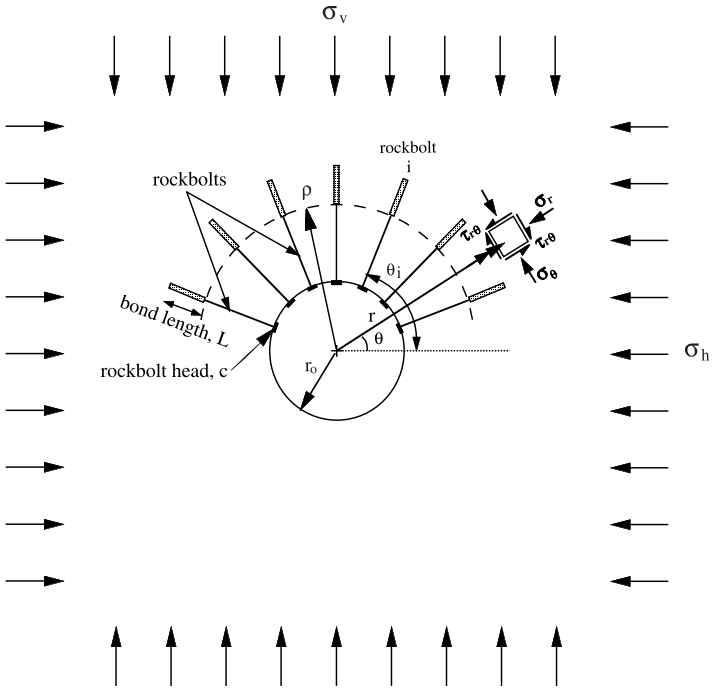

Fig. 3. Tunnel with point anchored rockbolts (the point anchor is represented by the bond length L)

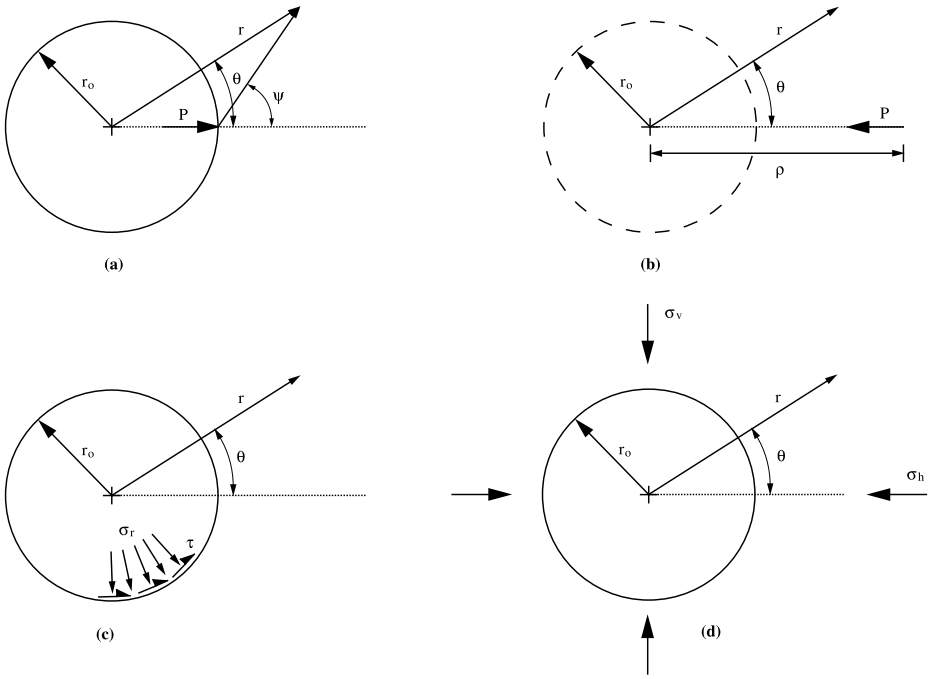

Fig. 4. Problem decomposition. (**a**) Problem I: concentrated load at tunnel perimeter; (**b**) Problem II: concentrated load in infinite medium; (**c**) Problem III: stress superposition at tunnel perimeter; (**d**) Problem IV: far field stresses

The rockbolts are considered as springs with load proportional to elongation. Thus a rockbolt can be replaced by a pair of concentrated loads of equal magnitude and opposite direction, one acting at the anchor head and the other one at the anchor point of the rockbolt. Since this is a 2D analysis, it is assumed that the rockbolt loads are distributed per unit length of tunnel. The singularity created by the concentrated loads at the ends of the rockbolts is removed by taking into account the actual geometry of the connection between the rockbolt and the ground; details are provided in the following sections. Because of elasticity, the problem can be decomposed into four different problems: Problem I: A concentrated load of magnitude P applied at the tunnel perimeter (Fig. 4a); Problem II: A concentrated load in an infinite medium (i.e. there is no tunnel) of magnitude P applied at a distance ρ (Fig. 4b); Problem III: A stress field applied at the tunnel perimeter of equal and opposite magnitude to the field produced by Problem II at the same location (Fig. 4c), such that superposition of Problems II and III would result in the solution of the problem of a concentrated load in the medium with a circular opening (i.e. the normal and shear stresses at the tunnel perimeter are zero); and Problem IV: a tunnel subjected to a far field stress σ_v and σ_h (Fig. 4d). Note that P in Fig. 4(a) and 4(b) is the load applied to the ground by the rockbolt; the load on the rockbolt is the same but with opposite magnitude. Thus for the ground the load P induces shortening while for the rockbolt induces elongation.

The complete solution can be obtained by the addition of the solutions of Problems I through IV. To obtain the loads on the rockbolts compatibility of deformations between the ground and each rockbolt must be imposed. Thus for rockbolt i (Fig. 3):

$$^{\mathrm{I}}\Delta U^i + {}^{\mathrm{II}}\Delta U^i + {}^{\mathrm{III}}\Delta U^i + {}^{\mathrm{IV}}\Delta U^i = \left(\frac{4S(\rho - r_o)}{\pi E_s (d_s)^2} P\right)^i = \left(\frac{P}{k}\right)^i, \tag{2}$$

where $\Delta U^i = U_r^i|_{r=\rho} - U_r^i|_{r=r_o}$. The left hand side of Eq. (2) corresponds to the elongation of rockbolt i due to the far field stresses and all the rockbolts, including rockbolt i itself. The right hand side of the equation is the elongation of the rockbolt shaft due to the load P (note that, as mentioned, the analysis assumes that the rockbolts loads are distributed per unit length of tunnel, thus the product of the load and the longitudinal rockbolt spacing is the actual load that the rockbolt carries), which can be expressed as the ratio between the load and the spring constant $k = \frac{\pi E_s (d_s)^2}{4S(\rho - r_o)}$. For a tunnel with N rockbolts, a linear system of N equations can be established with N unknowns which are the loads of the rockbolts. Note that the distribution of the rockbolts in the tunnel does not have to be symmetric. The following sections present the analytical solution for each problem.

2.1 Problem I: Concentrated Load at the Tunnel Perimeter

The geometry of the problem is illustrated in Fig. 4a. A solution for a similar case but in plane stress already exists (Timoshenko and Goodier, 1970). Unfortunately the solution does not satisfy strain compatibility in plane strain; for this reason a completely new solution has been developed. The Airy stress function, ϕ, in plane strain is (see Appendix II):

$$\phi = \frac{P}{\pi}\left[\psi r \sin\theta + \frac{1}{2} r_o \ln r - \frac{1}{2} r\theta \sin\theta - \frac{1-2\nu}{4(1-\nu)} r \ln r \cos\theta - \frac{3-4\nu}{8(1-\nu)} \frac{r_o^2}{r} \cos\theta\right] \tag{3}$$

This function satisfies equilibrium, strain compatibility, and boundary conditions. Stresses and displacements are given by:

$$\sigma_r = \frac{P}{\pi}\left\{\frac{2r\cos\theta - r_o(1+\cos^2\theta)}{(r - r_o\cos\theta)^2 + r_o^2 \sin^2\theta} + \frac{(r_o^2 - r^2) r_o \sin^2\theta}{\left[(r - r_o\cos\theta)^2 + r_o^2 \sin^2\theta\right]^2} + \frac{1}{2}\frac{r_o}{r^2} - \frac{5-6\nu}{4(1-\nu)}\frac{1}{r}\cos\theta + \frac{3-4\nu}{4(1-\nu)}\frac{r_o^2}{r^3}\cos\theta\right\}$$

$$\sigma_\theta = -\frac{P}{\pi}\left\{\frac{2(r_o - r\cos\theta) r_o^2 \sin^2\theta}{\left[(r - r_o\cos\theta)^2 + r_o^2 \sin^2\theta\right]^2} + \frac{1}{2}\frac{r_o}{r^2} + \frac{1-2\nu}{4(1-\nu)}\frac{1}{r}\cos\theta + \frac{3-4\nu}{4(1-\nu)}\frac{r_o^2}{r^3}\cos\theta\right\}$$

$$\tau_{r\theta} = \frac{P}{\pi}\left\{\frac{2r_o\sin\theta\cos\theta}{(r-r_o\cos\theta)^2+r_o^2\sin^2\theta} - \frac{2\,r\,r_o^2\sin^3\theta}{\left[(r-r_o\cos\theta)^2+r_o^2\sin^2\theta\right]^2} - \frac{1-2\nu}{4(1-\nu)}\frac{1}{r}\sin\theta + \frac{3-4\nu}{4(1-\nu)}\frac{r_o^2}{r^3}\sin\theta\right\} \tag{4}$$

$$\begin{aligned} U_r = -\frac{(1+\nu)P}{\pi E}\Bigg\{&(1-\nu)\cos\theta\ln\left[(r-r_o\cos\theta)^2+r_o^2\sin^2\theta\right] - \frac{5-12\nu+8\nu^2}{4(1-\nu)}\cos\theta\ln r \\ &-(1-2\nu)\sin\theta\left[\tan^{-1}\left(\frac{r-r_o\cos\theta}{r_o\sin\theta}\right)-\frac{\pi}{2}\mathrm{sign}(\theta)\right] \\ &+\frac{r\,r_o\sin^2\theta}{(r-r_o\cos\theta)^2+r_o^2\sin^2\theta} - \frac{1}{2}\frac{r_o}{r} - \frac{3-4\nu}{8(1-\nu)}\frac{r_o^2}{r^2}\cos\theta\Bigg\} \end{aligned}$$

$$\begin{aligned} U_\theta = \frac{(1+\nu)P}{\pi E}\Bigg\{&(1-\nu)\sin\theta\ln\left[(r-r_o\cos\theta)^2+r_o^2\sin^2\theta\right] - \frac{5-12\nu+8\nu^2}{4(1-\nu)}\sin\theta\ln r \\ &+(1-2\nu)\cos\theta\left[\tan^{-1}\left(\frac{r-r_o\cos\theta}{r_o\sin\theta}\right)-\frac{\pi}{2}\mathrm{sign}(\theta)\right] \\ &+\frac{1}{2}\frac{(r^2-r_o^2)\sin\theta}{(r-r_o\cos\theta)^2+r_o^2\sin^2\theta} - \frac{1-2\nu}{4(1-\nu)}\sin\theta + \frac{3-4\nu}{8(1-\nu)}\frac{r_o^2}{r^2}\sin\theta\Bigg\} \end{aligned} \tag{5}$$

The displacements, as expected, have a singularity at the point of application of the load ($r = r_o$, $\theta = 0$). This indicates that the local distribution of the load has a large

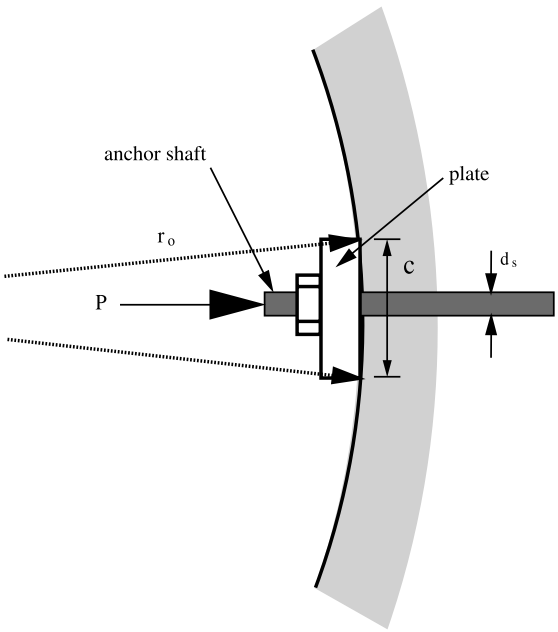

Fig. 5. Schematic of rockbolt head

influence on the displacement at this particular location. In practice the rockbolts' load is applied to the tunnel wall through a small but finite area (rockbolt head) that distributes the load; see Fig. 5. The size of the area along the perimeter of the tunnel is taken as c (side of the square, or diameter or the circular plate). Because of the plane strain assumption it is assumed that the load is distributed uniformly along the axis of the tunnel; this is a limitation of the model but it is necessary because of the 2D analysis. Integration of the displacements due to a distributed load of magnitude $\sigma = P/c$ over the area of the rockbolt head gives:

$$U_r\Big|_{\substack{r=r_o\\ \theta=0}} = -\frac{1+\nu}{1-\nu}\frac{P}{8\pi E}\left[-(3-4\nu)(5-4\nu) + 16(1-\nu)^2 \ln\left(\frac{c}{2r_o}\right) + 2(3-4\nu)\ln r_o\right]$$

$$U_\theta\Big|_{\substack{r=r_o\\ \theta=0}} = 0. \tag{6}$$

Stresses and displacements at locations other than the anchor head are not much affected by the local distribution of the load provided that c/r_o is small, which is generally the case. The errors introduced to other rockbolt elongations are smaller than about 1%.

2.2 Problem II: Concentrated Load in an Infinite Medium

The problem is shown in Fig. 4b. This is Kelvin's problem (Soutas-Little, 1999). For completeness the stresses and displacements are included. They are in polar coordinates:

$$\sigma_r = -\frac{P}{8\pi(1-\nu)}\left\{\frac{-2\rho + (7-4\nu)r\cos\theta - 4(1-\nu)\rho\cos 2\theta - r\cos 3\theta}{(r-\rho\cos\theta)^2 + \rho^2\sin^2\theta} - r^2\frac{\rho + r\cos\theta - 2\rho\cos 2\theta - r\cos 3\theta + \rho\cos 4\theta}{\left[(r-\rho\cos\theta)^2 + \rho^2\sin^2\theta\right]^2}\right\}$$

$$\sigma_\theta = -\frac{P}{8\pi(1-\nu)}\left\{\frac{-2\rho - (3-4\nu)r\cos\theta + 4(1-\nu)\rho\cos 2\theta + r\cos 3\theta}{(r-\rho\cos\theta)^2 + \rho^2\sin^2\theta} + r^2\frac{\rho + r\cos\theta - 2\rho\cos 2\theta - r\cos 3\theta + \rho\cos 4\theta}{\left[(r-\rho\cos\theta)^2 + \rho^2\sin^2\theta\right]^2}\right\}$$

$$\tau_{r\theta} = -\frac{P}{8\pi(1-\nu)}\left\{\frac{-(5-4\nu)r\sin\theta + 4(1-\nu)\rho\sin 2\theta + r\sin 3\theta}{(r-\rho\cos\theta)^2 + \rho^2\sin^2\theta} + r^2\frac{3r\sin\theta - 2\rho\sin 2\theta - r\sin 3\theta + \rho\sin 4\theta}{\left[(r-\rho\cos\theta)^2 + \rho^2\sin^2\theta\right]^2}\right\} \tag{7}$$

$$U_r = \frac{1+\nu}{1-\nu}\frac{P}{8\pi E}\left\{(3-4\nu)\cos\theta\ln\left[(r\cos\theta-\rho)^2 + r^2\sin^2\theta\right] + \frac{2r\rho\sin^2\theta}{(r\cos\theta-\rho)^2 + r^2\sin^2\theta}\right\}$$

$$U_\theta = -\frac{1+\nu}{1-\nu}\frac{P}{8\pi E}\left\{(3-4\nu)\sin\theta\ln\left[(r\cos\theta-\rho)^2 + r^2\sin^2\theta\right] + \frac{2(r-\rho\cos\theta)r\sin\theta}{(r\cos\theta-\rho)^2 + r^2\sin^2\theta}\right\} \tag{8}$$

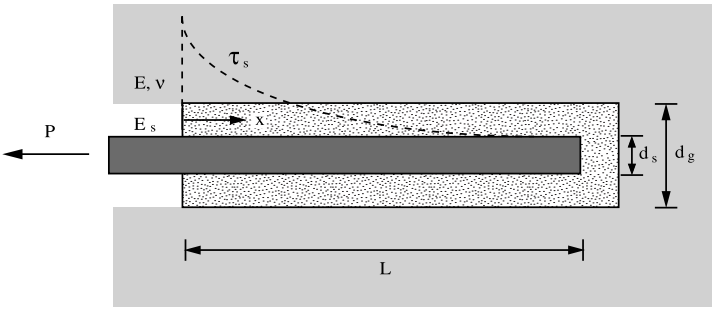

Fig. 6. Schematic of rockbolt bonded end (point anchor is represented by finite bonded length L; see text)

Because of the concentrated load, the displacements are singular at the point of application of the load ($r = \rho$, $\theta = 0$). Similar to Problem I the displacements at the anchor point of a rockbolt depend on the actual distribution of the load. Anchoring of rockbolts may be accomplished by mechanical means or by cementing a suitable length of the rockbolt (bond length in Fig. 3) to the surrounding ground. Figure 6 is an idealization of the bond zone between the rockbolt and the ground. The assumption is that the bond length L is much smaller than the anchor shaft length. The transfer of the rockbolt load, P, to the surrounding ground is a difficult problem and no exact solution exists. An approximate solution can be found using shear-lag analysis where the shape of the shear stress distribution between the rockbolt and the ground is assumed (Nairn, 1997; Nairn and Mendels, 2001). This approach has been often followed to solve problems concerning materials with inclusions (Abramento and Whittle, 1993, 1995a, b; Hsueh, 1988, 1990a; Ochiai et al., 1999), of which a rockbolt inside a rock mass is an example. Application of the shear-lag analysis to the grouted length of the rockbolt can be found elsewhere (Farmer, 1975; Hsueh, 1990b; Li and Stillborg, 1999; Li, 2000); details of the derivations are beyond the scope of this paper. The following is the solution proposed by Li and Stillborg (1999) which is somewhat more general than the solution proposed by Farmer (1975) and has shown good agreement with experiments:

$$\begin{aligned} \tau_s &= \frac{2P\alpha}{\pi d_s^2} e^{-2\alpha\frac{x}{d_s}}, \\ \alpha^2 &= \frac{2\,G\,G_g}{E_s\left[G\ln\frac{d_g}{d_s} + G_g\ln\frac{d_o}{d_g}\right]}, \\ dF &= \pi d_s \tau_s\, dx, \end{aligned} \tag{9}$$

where τ_s is the shear stress along the bonded length of the rockbolt; P is the force at the free end ($x = 0$ in Fig. 6); d_s is the diameter of the rockbolt; d_g is the diameter of the grout (bonding material); d_o is the size of the area of influence of the rockbolt, which can be estimated as $d_o = 10\ d_g$ (Li, 2000); G is the ground shear modulus; G_g is the grout (bonding material) shear modulus; E_s is the Young's modulus of the rockbolt; and dF is the force in the rockbolt inside the bonded zone due to the shear stress. The shape of the shear stress τ_s distribution is shown in Fig. 6. The shear stress is maximum at the free end and quickly decreases along the bond length, due to the negative exponent in Eq. (9).

A solution that represents the actual connection details between the rockbolt and the ground can then be obtained by integration of Eqs. (7) and (8) where P is replaced by dF from Eq. (9), with integration limits between $x = 0$ and $x = L$. Integration can be done either analytically, which is a very tedious process, or numerically. Within the range of typical ground and rockbolt properties and geometries (i.e. for $0.1 \leqslant 2\alpha/d_s \leqslant 50$), and assuming that the bond length is small ($L \ll \rho - r_o$), stresses and displacements can be approximated using a constant average shear stress distribution (τ_{average}) along a bonded length, L_{eq}. Two conditions are imposed to obtain τ_{average} and L_{eq}: (1) The resultant force of the constant shear stress distribution must be equal to the force P applied; and (2) the point of application of the resultant force of the constant distribution (i.e. at $1/2\ L_{eq}$) must coincide with the point of application of the resultant of the distribution given by (9). Thus,

$$\pi d_s\, \tau_{\text{average}}\, L_{eq} \frac{1}{S} = P$$

$$L_{eq} = 2\frac{\int_0^L \tau_s x\, dx}{\int_0^L \tau_s\, dx}. \tag{10}$$

The equivalent length is:

$$L_{eq} = \frac{2}{\beta}\frac{(\beta L + 1)e^{-\beta L} - 1}{e^{-\beta L} - 1}$$

$$\beta = \frac{2\alpha}{d_s}. \tag{11}$$

The errors introduced using τ_{average} and L_{eq} have been found well below 5% (after comparing results from numerical integration and from the approximation suggested). Integration of the radial displacements given in Eq. (8) for a constant distribution of shear stress along a grouted length L_{eq} gives:

$$\begin{aligned}
U_r = \frac{1+\nu}{1-\nu}\frac{P}{8\pi E L_{eq}} \Big\{ & (3-4\nu)\cos\theta L_{eq}\Big\{\ln\left[\left(r\cos\theta-\rho-L_{eq}\right)^2+r^2\sin^2\theta\right]-2\Big\} \\
& + \left[4(1-\nu)r\sin^2\theta-(3-4\nu)(r-\rho\cos\theta)\right]\ln\left[\frac{\left(r\cos\theta-\rho-L_{eq}\right)^2+r^2\sin^2\theta}{\left(r\cos\theta-\rho\right)^2+r^2\sin^2\theta}\right] \\
& +8(1-\nu)r\sin\theta\cos\theta\tan^{-1}\left[\frac{L_{eq}r\sin\theta}{\left(r\cos\theta-\rho\right)\left(r\cos\theta-\rho-L_{eq}\right)^2+r^2\sin^2\theta}\right]\Big\} \\
U_\theta = -\frac{1+\nu}{1-\nu}\frac{P}{8\pi E L_{eq}} \Big\{ & (3-4\nu)\sin\theta L_{eq}\Big\{\ln\left[\left(r\cos\theta-\rho-L_{eq}\right)^2+r^2\sin^2\theta\right]-2\Big\} \\
& -\left[(3-4\nu)(r\cos\theta-\rho)+r\cos\theta\right]\sin\theta\ln\left[\frac{\left(r\cos\theta-\rho-L_{eq}\right)^2+r^2\sin^2\theta}{\left(r\cos\theta-\rho\right)^2+r^2\sin^2\theta}\right] \\
& +8(1-\nu)r\sin^2\theta\tan^{-1}\left[\frac{L_{eq}\,r\sin\theta}{\left(r\cos\theta-\rho\right)\left(r\cos\theta-\rho-L_{eq}\right)^2+r^2\sin^2\theta}\right]\Big\}
\end{aligned} \tag{12}$$

For $r=\rho$ and $\theta=0$, the displacements are:

$$U_r\Big|_{\substack{r=\rho\\ \theta=0}} = \frac{(1+\nu)(3-4\nu)}{8\pi E(1-\nu)} 2P\big(\ln L_{eq} - 1\big)$$
$$U_\theta\Big|_{\substack{r=\rho\\ \theta=0}} = 0. \tag{13}$$

The stresses at $r=r_o$ are of particular interest, as will be shown in the next section. These stresses can be obtained with a small error using in Eqs. (7) $\rho_{eq}=\rho+L_{eq}/2$, provided that the length of the rockbolt is much larger than the bond length, which is generally the case for this type of rockbolts.

2.3 Problem III: Stress Superposition at Tunnel Perimeter

Problem II is concerned with a concentrated load in an infinite medium. This is not the case since there is an opening with radius r_o. The stress field found in Section 2.2 (Problem II) produces non-zero radial and shear stresses at the perimeter of the tunnel. The correct solution can be found by applying at the perimeter of the opening radial and shear stresses of the same magnitude and opposite sign (i.e. Eqs. (7) with opposite sign). There is no closed-form solution for such stress field applied at the perimeter of a circular opening inside an infinite medium. An approximate solution can be found by expressing the radial and shear stresses at the perimeter of the tunnel in a Fourier series form and then using Michell's solution (Soutas-Little, 1999). Michell's solution is expressed as follows:

$$\sigma_r = \frac{a_o}{r^2} - 2\frac{a_1}{r^3}\cos\theta - \sum_{n=2}^{\infty}\left[n(n+1)\frac{a_n}{r^{n+2}} + (n+2)(n-1)\frac{b_n}{r^n}\right]\cos n\theta$$
$$\sigma_\theta = -\frac{a_o}{r^2} + 2\frac{a_1}{r^3}\cos\theta + \sum_{n=2}^{\infty}\left[n(n+1)\frac{a_n}{r^{n+2}} + (n-2)(n-1)\frac{b_n}{r^n}\right]\cos n\theta$$
$$\tau_{r\theta} = -2\frac{a_1}{r^3}\sin\theta - \sum_{n=2}^{\infty}\left[n(n+1)\frac{a_n}{r^{n+2}} + n(n-1)\frac{b_n}{r^n}\right]\sin n\theta$$
$$U_r = -\frac{1+\nu}{E}\left\{-\frac{a_o}{r} + \frac{a_1}{r^2}\cos\theta + \sum_{n=2}^{\infty}\left[n\frac{a_n}{r^{n+1}} + (n+2-4\nu)\frac{b_n}{r^{n-1}}\right]\cos n\theta\right\}$$
$$U_\theta = -\frac{1+\nu}{E}\left\{\frac{a_1}{r^2}\sin\theta + \sum_{n=2}^{\infty}\left[n\frac{a_n}{r^{n+1}} + (n-4+4\nu)\frac{b_n}{r^{n-1}}\right]\sin n\theta\right\} \tag{14}$$

The coefficients of Eq. (14) can be found from the Fourier series terms. The algebra is quite tedious, but finally the coefficients are given by Eqs. (15). Note that stresses and displacements in Eqs. (14) are given by an infinite series of terms. As expected the results improve with the number of terms used; for practical purposes a good approximation can be found using only several terms.

$$a_o = \frac{2Pr_o^2}{8\pi(1-\nu)}\frac{1}{\left(r_o^2-\rho_{eq}^2\right)^3}\left[\frac{1}{\rho_{eq}}\left(\rho_{eq}^6 - r_o^6\right) - 3\rho_{eq}r_o^2\left(\rho_{eq}^2 - r_o^2\right)\right]$$

$$a_1 = -\frac{1}{4}\frac{r_o^2}{\rho_{eq}}a_o$$

$$a_n = \frac{Pr_o^{n+2}}{8\pi(1-\nu)}\frac{1}{\left(r_o^2-\rho_{eq}^2\right)^3}\left(\frac{r_o}{\rho_{eq}}\right)^{n-2}\left[-\frac{n}{n+1}\frac{1}{\rho_{eq}^3}\left(\rho_{eq}^8-r_o^8\right)\right.$$
$$+\frac{1}{n}\left(4n-4\nu-\frac{n-2}{n+1}\right)\frac{1}{\rho_{eq}}\left(\rho_{eq}^6-r_o^6\right)-\frac{3}{n}\left(2n-4\nu+\frac{n+2}{n+1}\right)\rho_{eq}\left(\rho_{eq}^4-r_o^4\right)$$
$$\left.+\frac{1}{n}\left(4n-12\nu+\frac{5n+6}{n+1}\right)\rho_{eq}^3\left(\rho_{eq}^2-r_o^2\right)\right]$$

$$b_n = \frac{Pr_o^n}{8\pi(1-\nu)}\frac{1}{\left(r_o^2-\rho_{eq}^2\right)^3}\left(\frac{r_o}{\rho_{eq}}\right)^{n-2}\left[\frac{1}{\rho_{eq}^3}\left(\rho_{eq}^8-r_o^8\right)-\frac{4n-4\nu-1}{n-1}\frac{1}{\rho_{eq}}\left(\rho_{eq}^6-r_o^6\right)\right.$$
$$\left.+\frac{3(2n-4\nu+1)}{n-1}\rho_{eq}\left(\rho_{eq}^4-r_o^4\right)-\frac{4n-12\nu+5}{n-1}\rho_{eq}^3\left(\rho_{eq}^2-r_o^2\right)\right]$$

$$\rho_{eq} = \rho + \frac{L_{eq}}{2} \tag{15}$$

2.4 Problem IV: Far Field Stresses

The stress and displacement fields produced around a circular opening are (Hoek and Brown, 1982):

$$\sigma_r = \frac{1}{2}(\sigma_v+\sigma_h)\left[1-\left(\frac{r_o}{r}\right)^2\right]-\frac{1}{2}(\sigma_v-\sigma_h)\left[1-4\left(\frac{r_o}{r}\right)^2+3\left(\frac{r_o}{r}\right)^4\right]\cos 2\theta$$

$$\sigma_\theta = \frac{1}{2}(\sigma_v+\sigma_h)\left[1+\left(\frac{r_o}{r}\right)^2\right]+\frac{1}{2}(\sigma_v-\sigma_h)\left[1+3\left(\frac{r_o}{r}\right)^4\right]\cos 2\theta$$

$$\tau_{r\theta} = \frac{1}{2}(\sigma_v-\sigma_h)\left[1+2\left(\frac{r_o}{r}\right)^2-3\left(\frac{r_o}{r}\right)^4\right]\sin 2\theta$$

$$U_r = -\frac{1+\nu}{E}\left\{\frac{1}{2}(\sigma_v+\sigma_h)\frac{r_o^2}{r}-\frac{1}{2}(\sigma_v-\sigma_h)\left[4(1-\nu)\frac{r_o}{r}-\left(\frac{r_o}{r}\right)^3\right]r_o\cos 2\theta\right\}$$

$$U_\theta = -\frac{1+\nu}{E}\frac{1}{2}(\sigma_v-\sigma_h)\left[2(1-2\nu)\frac{r_o}{r}+\left(\frac{r_o}{r}\right)^3\right]r_o\sin 2\theta \tag{16}$$

Note that Eqs. (16) reflect only the ''net'' displacements, which are produced by the far field stresses after excavation (Einstein and Schwartz, 1979). Only ''net'' displacements must be included in the formulation since these are the displacements that will affect the rockbolts since they are placed after excavation. The initial displacements originated by the constant far field stress, σ_v and σ_h, do not affect the solution.

2.5 Implementation of the Analytical Solution

The total displacements at a particular point are obtained by the addition of the displacements found from the solution of Problems I through IV. Note that the origin

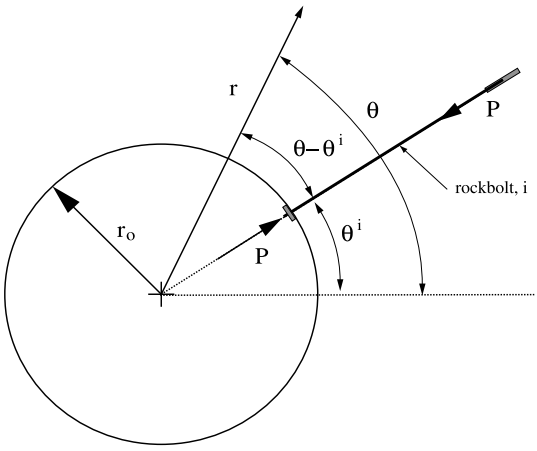

Fig. 7. Global and local polar coordinate system

of angles used in Problems I through III corresponds to the direction of the rockbolt, and thus the angular coordinates are expressed on a local coordinate system; in other words, if a point has as a global angular coordinate θ (the global angular coordinate is measured from the horizontal and is positive counterclockwise; see Fig. 7), the angle that must be used in Eqs. (3) to (12) is $\theta - \theta^i$ where θ^i is the global angular coordinate of the direction of rockbolt i (Fig. 7).

Compatibility of displacements between rockbolt and ground is satisfied using Eq. (2). The first term on the left hand side of the equation (${}^{\mathrm{I}}\Delta U^i$) is found from Eqs. (5) if $r \neq r_o$ and $\theta \neq 0$; otherwise Eqs. (6) should be used. The second term (${}^{\mathrm{II}}\Delta U^i$) is found from (11) if $r \neq \rho$ and $\theta \neq 0$; otherwise Eqs. (12) apply. The other two terms (${}^{\mathrm{III}}\Delta U^i$, ${}^{\mathrm{IV}}\Delta U^i$) are obtained from (13) and (15), respectively. Pre-stressed rockbolts, with initial load P_o, can be considered by replacing P with $P_o - P$ on the right hand side of Eq. (2). The final load on the rockbolt is P if $P > P_o$; otherwise it is the initial load P_o.

Equation (2) is repeated for each rockbolt, from $i = 1$ to N. As a result a linear system of equations is obtained with a solution that is the load carried by each rockbolt. Stresses and displacements can then be obtained by using the actual loads in the equations previously derived. The process described can be automated with a computer program.

Inspection of all the terms in Eq. (2) shows that the solution depends only on the following non-dimensional parameters: k_o, ν, r_o/ρ, c/r_o, ρ_{eq}/ρ, E/E_s, and $Sr_o/(d_s)^2$; the last two parameters can be grouped into k/E, the ratio between the rockbolt spring constant and the Young's modulus of the ground; note that from Eq. (2), $k/E = \frac{E_s}{E}\frac{\pi(d_s)^2}{4Sr_o(\rho/r_o - 1)}$. The following example illustrates the results obtained from the analytical solution. The parameters used are: $k_o = 0.5$; $\nu = 0.2$; $r_o/\rho = 0.33$; $c/r_o = 0.075$; $\rho_{eq}/\rho = 1.025$; and $Sr_o/(d_s)^2 = 4.44 \times 10^3$. Seven rockbolts are placed at 45°, 60°, 75°, 90°, 105°, 120°, and 135° (i.e. a symmetric distribution around the crown of the tunnel with the rockbolts spaced 15°) and are spaced every two meters

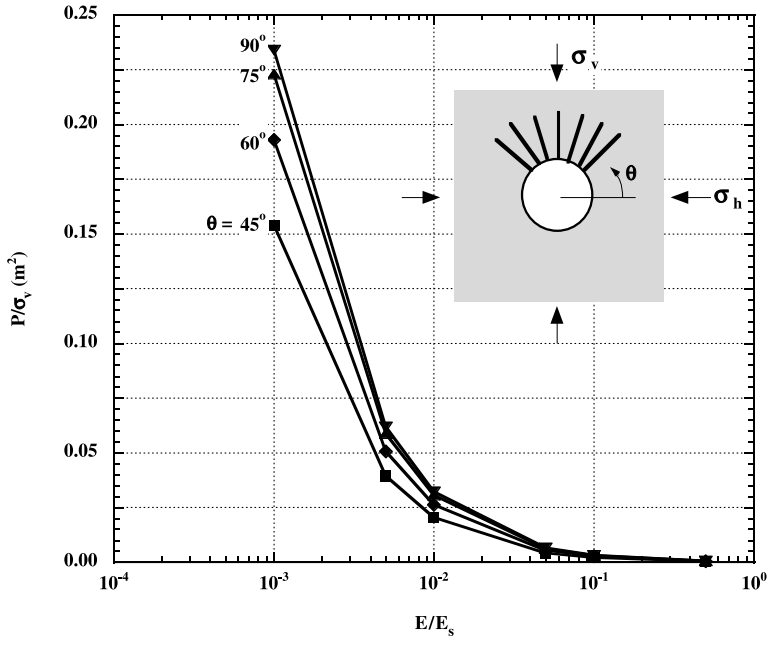

Fig. 8. Point anchored rockbolt loads P/σ_v versus relative stiffness E/E_s. Input parameters: $k_o = 0.5$; $\nu = 0.2$; $r_o/\rho = 0.33$; $c/r_o = 0.075$; $\rho_{eq}/\rho = 1.025$; $Sr_o/(d_s)^2 = 4.44 \times 10^3$

along the axis of the tunnel. Figure 8 shows the load on the rockbolts as a function of the relative stiffness between the rockbolts and the ground defined in this case by the ratio of the Young's modulus of the two materials. As expected the loads decrease with increasing the stiffness of the ground relative to the rockbolts. The rockbolt placed at the crown ($\theta = 90°$) carries the largest load and the rockbolt at mid height ($\theta = 45°$) the smallest. This is reasonable because the far-field horizontal stress is smaller than the vertical stress, and thus a larger unloading (and as a consequence large deformation) occurs at the crown. The differences of rockbolts' loads decrease as the stiffness of the ground and rockbolts becomes similar.

The same example is solved with the FEM ABAQUS where the rockbolts are modeled as springs with the end-points one at the perimeter of the tunnel and the other one at the anchor point. About 5,400 8-node isoparametric elements have been used for the discretization. The numerical method should consider the geometry of the anchor head and the grouted end of the rockbolts to avoid the problems derived by the concentrated loads (see Fig. 2). Otherwise the results obtained would not be realistic and the solution would depend on the discretization used. Addition of the connection details into the discretization would introduce such a high level of complexity for the modeling and ensuing numerical solution that it is unrealistic to expect that such refinement would be included in routine calculations. As a practical alternative it is proposed to use in the numerical model an "equivalent" spring constant, k_{eq}, for each rockbolt that includes the contributions of the end effects. The equivalent spring constant depends on the discretization used (see Fig. 2), properties of the

materials, and geometry of the problem, but not on the loading imposed due to the assumption of elasticity. Thus the equivalent spring constant for each rockbolt should be computed using the same discretization, properties, and geometry, as the problem to be solved, but not necessarily using the same loading. The equivalent spring constant has then been obtained by matching the results of a new FE analysis with the analytical solution for a simpler loading, using in both cases the same geometry, mesh, and properties, but with $k_o = 1$ ($\sigma_v = \sigma_h$). Since all rockbolts in the example are identical, the new analysis has been carried out with only one rockbolt. The spring constant k input into the model is modified until the load obtained with the FEM is identical to the load obtained with the analytical solution (the iterations were finished when the differences were smaller than 10%). Equivalent spring constants are obtained following the procedure described for each of the relative stiffnesses in Fig. 8.

Figure 9 shows the rockbolts' loads obtained with the FEM using the equivalent spring constant and how the loads compare with the analytical solution. It can be observed that the comparison is very good, with errors less than 10%. The figure also shows the ratio between the equivalent spring constant, k_{eq}, and the actual spring constant, k. The ratio is about one for large relative stiffness (E/E_s ratio), which indicates stiff ground, and increases quickly as the ground becomes softer. Note that this observation compares well with the results shown in Fig. 2, which indicate that the rockbolt load is relatively insensitive to the discretization for relatively stiff ground. Figure 10 is a comparison of the radial displacements obtained with the FEM and with

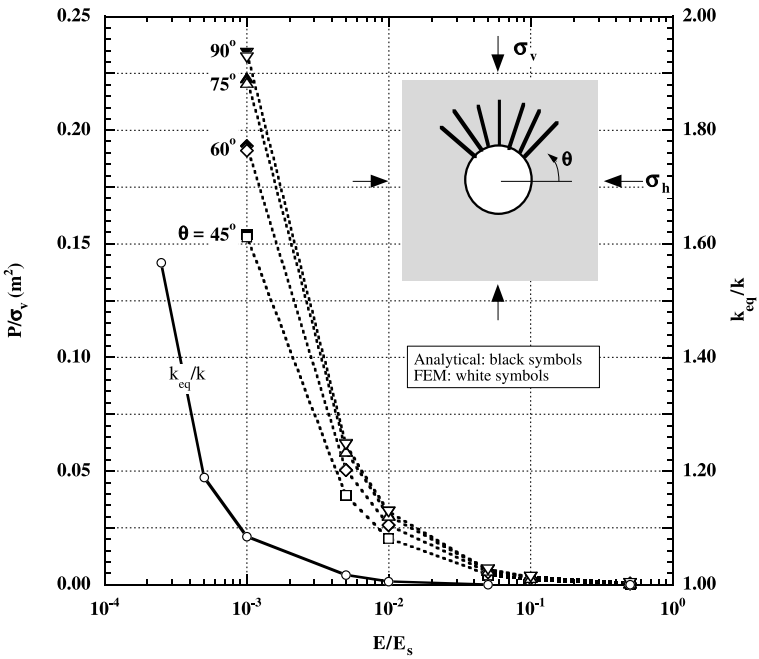

Fig. 9. Point anchored rockbolt loads P/σ_v and equivalent and actual rockbolt spring constant ratio k_{eq}/k versus relative stiffness E/E_s. Comparison between finite element method and analytical solution. Input parameters: $k_o = 0.5$; $\nu = 0.2$; $r_o/\rho = 0.33$; $c/r_o = 0.075$; $\rho_{eq}/\rho = 1.025$; $Sr_o/(d_s)^2 = 4.44 \times 10^3$

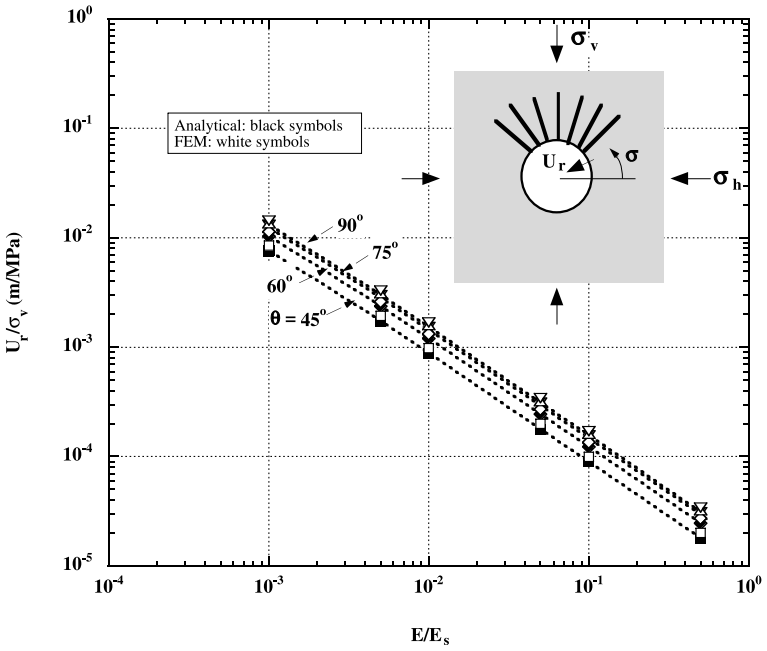

Fig. 10. Point anchored rockbolt head displacements U_r/σ_v versus relative stiffness E/E_s. Comparison between finite element method and analytical solution. Input parameters: $k_o = 0.5$; $\nu = 0.2$; $r_o/\rho = 0.33$; $c/r_o = 0.075$; $\rho_{eq}/\rho = 1.025$; $Sr_o/(d_s)^2 = 4.44 \times 10^3$

the analytical solution using the equivalent spring constant. The results compare very well (results from the analytical and FEM solutions fall on top of each other in the Figure).

The importance of the different factors on the rockbolts' loads has been investigated through a parametric study. Figure 11 is a plot of the normalized load on a single rockbolt for different relative stiffness (E/E_s) and different relative rockbolt length (r_o/ρ). The other parameters have been kept constant and equal to: $k_o = 1$; $\nu = 0.2$; $c/r_o = 0.1$; $\rho_{eq}/\rho = 1.1$; and $Sr_o/(d_s)^2 = 2 \times 10^4$. The figure shows that the load has an almost linear dependency on relative stiffness, with the load getting smaller as the ground gets comparatively stiffer. The figure also shows that as the length of the rockbolt increases, the load decreases. This is due to two factors that have opposite effects: on the one hand as the distance between the anchor head and anchor point increases, the displacements between the two points induced by the opening increase; on the other hand, as the rockbolt gets longer, it has smaller strains for the same elongation. In the case shown in Fig. 11, the second factor takes precedence and thus the load on the rockbolt decreases as it becomes longer.

The importance of the other parameters has been investigated by comparing the loads obtained when changing one of the parameters with the load from a reference case (base case). The base case has the following characteristics: $k_o = 1$; $\nu = 0.2$; $E/E_s = 0.025$; $r_o/\rho = 0.5$; $c/r_o = 0.1$; $\rho_{eq}/\rho = 1.1$, and $Sr_o/(d_s)^2 = 2 \times 10^4$. Figure 12 is a plot of the ratio between the load obtained for different values of ν, c/r_o, and

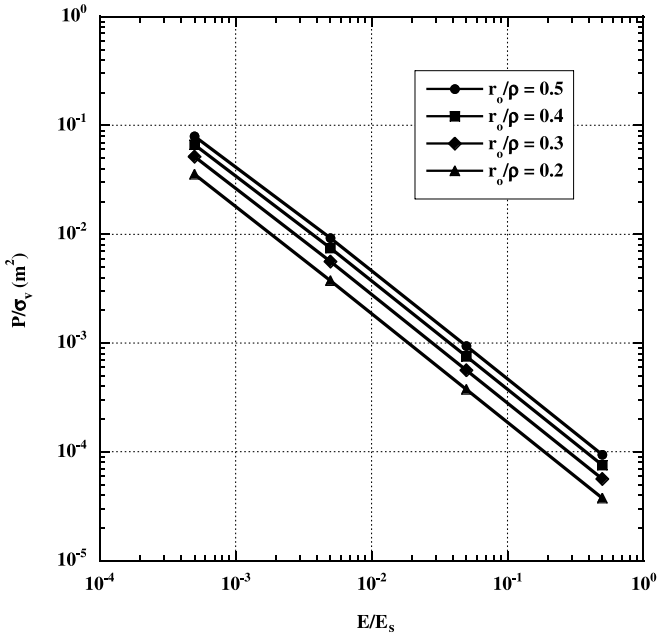

Fig. 11. Point anchored rockbolt load P/σ_v versus relative stiffness E/E_s and length r_o/ρ. Input parameters: $k_o = 1.0$; $\nu = 0.2$; $c/r_o = 0.1$; $\rho_{eq}/\rho = 1.1$; $Sr_o/(d_s)^2 = 2.0 \times 10^4$

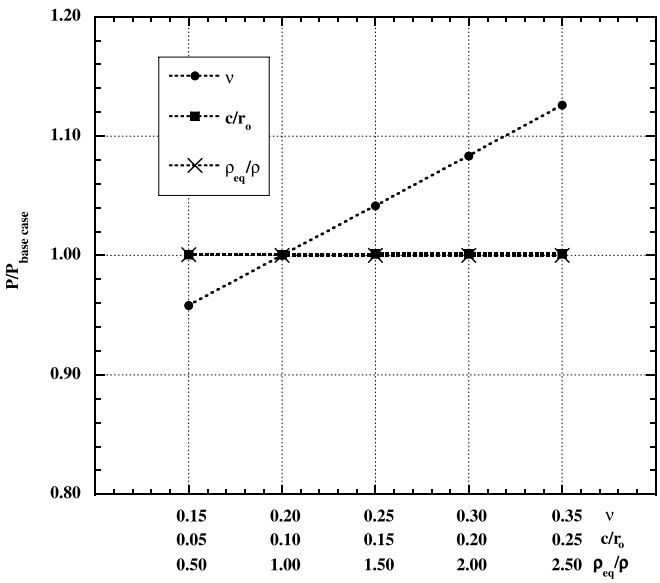

Fig. 12. Point anchored rockbolt load $P/P_{\text{base case}}$ versus Poisson's ratio ν, anchor head size c/r_o, and bond length ρ_{eq}/ρ. Input parameters:. $k_o = 1.0$; $E/E_s = 0.025$; $r_o/\rho = 0.5$; $Sr_o/(d_s)^2 = 2.0 \times 10^4$. Base case with: $\nu = 0.2$; $c/r_o = 0.1$; $\rho_{eq}/\rho = 1.1$

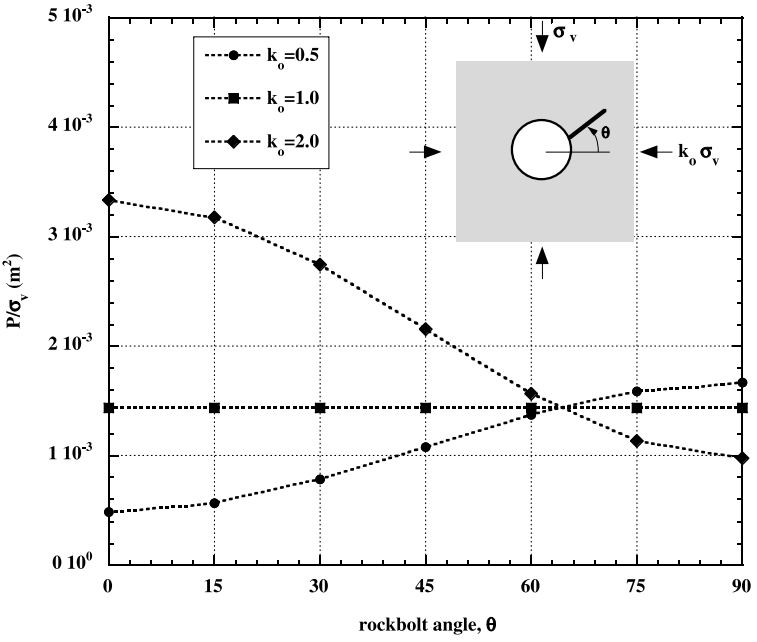

Fig. 13. Point anchored rockbolt load P/σ_v versus coefficient of earth pressure at rest k_o, and orientation θ. Input parameters: $k_o = 1.0$; $\nu = 0.2$; $E/E_s = 0.025$; $r_o/\rho = 0.5$; $c/r_o = 0.1$; $\rho_{eq}/\rho = 1.1$; $Sr_o/(d_s)^2 = 2.0 \times 10^4$

ρ_{eq}/ρ and the base case. The figure shows the small effect of all three parameters. A modest increase of load occurs with the Poisson's ratio: about 10% with a twofold increase of ν; the effect of the other two parameters is negligible.

The effect of k_o can be observed in Fig. 13, which is a plot of the normalized load with the orientation of the rockbolt and with the magnitude of k_o. As expected the load is independent of the location of the rockbolt for $k_o = 1$ due to the symmetry of the problem. The largest loads are at the crown ($\theta = 90°$) for $k_o = 0.5$ and at the springline ($\theta = 0°$) for $k_o = 2$, which coincide with the directions of the largest unloading after excavation.

3. Conclusions

A new analytical solution for the analysis of point anchored rockbolts as tunnel support has been developed and presented in the paper. The following assumptions are made: elastic response of ground and rockbolts; deep tunnel with circular cross section; plane strain conditions. The solution includes details of the geometry of the head and bonded length of the rockbolt. It has been shown that these details are critical to obtain an accurate solution. In fact, results obtained with numerical analyses where rockbolts are modeled as concentrated loads may be inaccurate and may strongly depend on the discretization employed. The error increases with decreasing stiffness of the ground relative to the stiffness of the rockbolt. Since this is a displacement-

driven problem the magnitude of the rockbolts' load is particularly sensitive to discretization and connection details. As a consequence modeling of rockbolts as concentrated loads or springs should be done only for tunnels in stiff ground; otherwise the connections should be explicitly included in the model.

An alternative that is cost-effective is to include the rockbolts in the numerical model as springs with an ''equivalent'' spring constant that includes end effects. The equivalent spring constant can be obtained by matching the numerical results with the analytical solution for a simple problem. The spring constant can then be used with more complex models.

The analytical solution obtained shows that the load on a single rockbolt depends on a number of non-dimensional variables, namely k_o, ν, E/E_s, r_o/ρ, c/r_o, ρ_{eq}/ρ, and $Sr_o/(d_s)^2$, of which the most important one is E/E_s, the relative stiffness between the ground and the rockbolt. The analytical solution is easy to use, incorporates the fundamental variables, and provides an accurate magnitude of the rockbolts' loads for the conditions assumed in the formulation (i.e. linear elasticity, deep tunnel, plane strain). It cannot substitute detailed numerical models due to the limitations of some of the assumptions made.

References

Abramento, M., Whittle, A. J. (1993): Shear-lag analysis of a planar soil reinforcement in plane strain compression. J. Engng. Mech. ASCE 119(2), 270–291.

Abramento, M., Whittle, A. J. (1995a): Analysis of pullout tests for planar reinforcements in soil. J. Geotechn. Engng. ASCE 121(6), 476–485.

Abramento, M., Whittle, A. J. (1995b): Experimental evaluation of pullout analyses for planar reinforcements. J. Geotechn. Engng. ASCE 121(6), 486–492.

Alonso, E., Alejano, L. R., Varas, F., Fdez-Manín, G., Carranza-Torres, C. (2003): Ground response curves for rock masses exhibiting strain-softening behaviour. Int. J. Numer. Anal. Methods Geomech. 27, 1153–1185.

Aristorenas, G. (1992): Time dependent behavior of tunnels excavated in shale. Ph.D. Thesis, Massachusetts Institute of Technology, Cambridge, UA.

Augarde, C. E., Burd, H. J. (2001): Three-dimensional finite element analysis of lined tunnels. Int. J. Numer. Anal. Methods Geomech. 25, 243–262.

Bobet, A. (2001): Analytical solutions for shallow tunnels in saturated ground. ASCE J. Engng. Mech. 127(12), 1258–1266.

Bobet, A. (2002): Mechanically anchored rockbolts in tunnels in saturated ground. Proc. North American Rock Mechanics Symposium: NARMS-TAC 2002, 797–804.

Bobet, A. (2003): Effect of pore water pressure on tunnel support during static and seismic loading. Tunnel. Underground Space Technol. 18, 377–393.

Bobet, A., Aristorenas, G., Einstein, H. H. (1998): Feasibility analysis for a radioactive waste repository tunnel. Tunnel. Underground Space Technol. 13(4), 409–426.

Cai, Y., Esaki, T., Jiang, Y. (2004a): A rock bolt and rock mass interaction model. Int. J. Rock Mech. Min. Sci. 41, 1055–1067.

Cai, Y., Esaki, T., Jiang, Y. (2004b): An analytical model to predict axial load in grouted rock bolt for soft rock tunneling. Tunnel. Underground Space Technol. 19(6), 607–618.

Carranza, C., Fairhurst, C. (2000): Application of the convergence-confinement method of tunnel design to rock masses that satisfy the Hoek-Brown failure criterion. Tunnel. Underground Space Technol. 15(2), 187–213.

Chen, S.-H., Qiang, S., Chen, S.-F., Egger, P. (2004): Composite element model of the fully grouted rock bolt. Rock Mech. Rock Engng. 37(3), 193–212.

Eberhardt, E. (2001): Numerical modelling of three-dimension stress rotation ahead of an advancing tunnel face. Int. J. Rock Mech. Min. Sci. 38, 499–518.

Einstein, H. H., Schwartz, C. W. (1979): Simplified analysis for tunnel supports. J. Geotechn. Engng. Div. ASCE 105(GT4), 499–518.

Einstein, H. H., Bobet, A. (1997): Mechanized tunnelling in squeezing ground – from basic thoughts to continuous tunnelling. Proc. World Tunnel Congress '97. Vienna, Austria, 619–632.

Farmer, I. W. (1975): Stress distribution along resin grouted rock anchor. Int. J. Rock Mech. Min. Sci. Geomech. Abstr. 12, 347–351.

Gioda, G., Swoboda, G. (1999): Developments and applications of the numerical analysis of tunnels in continuous media. Int. J. Numer. Anal. Methods Geomech. 23, 1393–1405.

Grasselli, G. (2005): 3D Behaviour of bolted rock joints: experimental and numerical study. Int. J. Rock Mech. Min. Sci. 42, 13–24.

Hibbit, Karlson & Sorensen, Inc. (2002): ABAQUS/Standard User's Manual, Version 6-3.5, 1080 Main Street, Pawtucket, RI, USA.

Hoek, E., Brown, E. T. (1982): Underground excavations in rock. The Institution of Mining and Metallurgy, London.

Hsueh, C. H. (1988): Elastic load transfer from partially embedded axially loaded fibre to matrix. J. Mater. Sci. Lett. 7, 497–500.

Hsueh, C. H. (1990a): Interfacial debonding and fiber pull-out stresses of fiber-reinforced composites. Mater. Sci. Engng. A123, 1–11.

Hsueh, C. H. (1990b): Effects of interfacial bonding on sliding phenomena during compressive loading of an embedded fibre. J. Mater. Sci. 25, 4080–4086.

Kasper, T., Meschke, G. (2004): A 3D finite element simulation model for TBM tunnelling in soft ground. Int. J. Numer. Anal. Methods Geomech. 28, 1441–1460.

Kawamoto, T., Aydan, Ö. (1999): A review of numerical analysis of tunnels in discontinuous rock masses. Int. J. Numer. Anal. Methods Geomech. 23, 1377–1391.

Labiouse, V. (1996): Ground response curves for rock excavations supported by ungrouted tensioned rockbolts. Rock Mech. Rock Engng. 29(1), 19–38.

Lee, I., Nam, S. (2004): Effect of tunnel advance rate on seepage forces acting on the underwater tunnel face. Tunnel. Underground Space Technol. 19, 273–281.

Li, C. (2000): Analytical study of the behavior of rock bolts. In: Girard, J., Liebman, H., Breeds, C., Doe, T. (eds.), Proc., Pacific Rocks 2000. Balkema, Rotterdam.

Li, C., Stillborg, B. (1999): Analytical models for rock bolts. Int. J. Rock Mech. Min. Sci. Geomech. Abstr. 36, 1013–1029.

Liu, B., Yue, Z. Q., Tham, L. G. (2005): Analytical design method for a truss-bolt system for reinforcement of fractured coal mine roofs – illustrated with a case study. Int. J. Rock Mech. Min. Sci. 42, 195–218.

Muniz de Farias, M., Henrique, A., Pacheco, A. (2004): Displacement control in tunnels excavated by the NATM: 3-D numerical simulations. Tunnel. Underground Space Technol. 19, 283–293.

Nairn, J. A. (1997): On the use of shear-lag methods for analysis of stress transfer in unidirectional composites. Mech. Mater. 26, 63–80.

Nairn, J. A., Mendels, D. A. (2001): On the use of planar shear-lag methods for stress-transfer analysis of multilayered composites. Mech. Mater. 33, 335–362.

Ochiai, S., Hojo, M., Inoue, T. (1999): Shear-lag simulation of the progress of interfacial debonding in unidirectional composites. Composites Sci. Technol. 59, 77–88.

Oreste, P. P., Peila, D. (1996): Radial passive rockbolting in tunnelling design with a new onvergence-confinement model. Int. J. Rock Mech. Min. Sci. Geomech. Abstr. 33(5), 443–454.

Potyondy, D. O., Cundall, P. A. (2004): A bonded-particle model for rock. Int. J. Rock Mech. Min. Sci. 41, 1329–1364.

Serrano, A., Olalla, C. (1999): Tensile resistance of rock anchors. Int. J. Rock Mech. Min. Sci. Geomech. Abstr. 36, 449–474.

Shalabi, F. I. (2005): FE analysis of time-dependent behavior of tunneling in squeezing ground using two different creep models. Tunnell. Underground Space Technol. 20, 271–279.

Sharma, K. G., Pande, G. N. (1988): Stability of rock masses reinforced by passive, fully-grouted rock bolts. Int. J. Rock Mech. Min. Sci. Geomech. Abstr. 25(5), 273–285.

Sinha, R. S. (1989): Design methods. In: Sinha, R. S. (ed.), Underground structures: design and instrumentation, Elsevier Science Publishers, Amsterdam, pp 33–83.

Soutas-Little, R. V. (1999): Elasticity. Dover Publications, Inc, N.Y.

Stille, H., Holmberg, M., Nord, G. (1989): Support of weak Rock with grouted bolts and shotcrete. Int. J. Rock Mech. Min. Sci. Geomech. Abstr. 26(1), 99–113.

Suwansawat, V. (1998): Using the Relative Stiffness Method (Tunnelliner) and the Finite-Element Method (PLAXIS) for tunnel design. MIT Internal Report, Cambridge.

Tannant, D. D., Brummer, R. K., Yi, X. (1995): Rockbolt behaviour under dynamic loading: field tests and modelling. Int. J. Rock Mech. Min. Sci. Geomech. Abstr. 32(6), 537–550.

Timoshenko, S. P., Goodier, J. N. (1970): Theory of elasticity. 3rd edn., McGraw, New York.

Windsor, C. R. (1997): Rock reinforcement systems. Int. J. Rock Mech. Min. Sci. Geomech. Abstr. 34(6), 919–951.

Zhu, W., Li, S., Li, S., Chen, W., Lee, C. F. (2003): Systematic numerical simulation of rock tunnel stability considering different rock conditions and construction effects. Tunnell. Underground Space Technol. 18, 531–536.

Appendix I: Notation

c^i	anchor head dimension of rockbolt i
$d_s{}^i$	diameter of rockbolt i
E, ν	Young's modulus and Poisson's ratio of the ground
$E_s{}^i$	Young's modulus of rockbolt i
i	rockbolt number, from 1 to N
k_o	coefficient of earth pressure at rest; $k_o = \sigma_h/\sigma_v$
k^i	spring constant of rockbolt i
$k_{eq}{}^i$	equivalent spring constant of rockbolt i
L^i	anchored length of rockbolt i
L_{eq}	equivalent bonded length of rockbolt i
N	total number of rockbolts in the tunnel
P^i	axial load of rockbolt i

r, θ	polar coordinates
θ^i	angular coordinate of rockbolt i, measured from horizontal
r_o	tunnel radius
ρ^i	length of rockbolt i, measured from the center of the tunnel
${\rho_{eq}}^i$	equivalent length of rockbolt i
S^i	spacing of rockbolt i along tunnel axis
σ_v, σ_h	far field vertical and horizontal stresses
σ_r, σ_θ, $\tau_{r\theta}$	stresses in polar coordinates
τ_s	shear stress along the bonded length of the rockbolt
U_r, U_θ	displacements in polar coordinates

Appendix II: Concentrated Load in a Plane Strain Elastic Infinite Medium

An Airy stress function with a structure similar to that for plane stress is chosen (Timoshenko and Goodier, 1970):

$$\phi = \mathrm{A}\,\psi\, r\sin\theta + \mathrm{B}\ln r + \mathrm{C}\, r\theta\sin\theta + \mathrm{D}\, r\ln r\cos\theta + \mathrm{F}\, r^{-1}\cos\theta \qquad \text{(AII.1)}$$

where ϕ is the Airy stress function, A, B, C, D, and F are constants that will be obtained from boundary conditions, r and θ are polar coordinates (Fig. 4(a)), and ψ is an auxiliary angle, which is defined in Fig. 4(a). From the Airy stress function, stresses can be obtained with:

$$\begin{aligned}\sigma_r &= \frac{1}{r}\frac{\partial\phi}{\partial r} + \frac{1}{r^2}\frac{\partial^2\phi}{\partial\theta^2}\\ \sigma_\theta &= \frac{\partial^2\phi}{\partial r^2}\\ \tau &= -\frac{\partial}{\partial r}\left(\frac{1}{r}\frac{\partial\phi}{\partial\theta}\right).\end{aligned} \qquad \text{(AII.2)}$$

Strain compatibility is given by:

$$\gamma_{r\theta} = \frac{\partial U_\theta}{\partial r} - \frac{1}{r}U_\theta + \frac{1}{r}\frac{\partial U_r}{\partial\theta}. \qquad \text{(AII.3)}$$

Equation (AII.3) requires:

$$(1-2\nu)(A + C + D) = -D. \qquad \text{(AII.4)}$$

The boundary conditions are:

$$\begin{aligned}&\sigma_r = \sigma_\theta = \tau = 0, \quad \text{for } r \to \infty\\ &\sigma_r = \tau = 0, \qquad\quad \text{for } r = r_o.\end{aligned} \qquad \text{(AII.5)}$$

The first condition in Eq. (AII.5) is satisfied, given the Airy stress function chosen. The second condition is satisfied if:

$$\begin{aligned}B &= \frac{1}{2}r_o A\\ C &= -\frac{1}{2}A\\ D - 2\frac{F}{r_o^2} &= \frac{1}{2}A.\end{aligned} \qquad \text{(AII.6)}$$

Combining Eqs. (AII.4) and (AII.6), one gets:

$$B = \frac{1}{2} r_o A$$
$$C = -\frac{1}{2} A$$
$$D = -\frac{1-2\nu}{4(1-\nu)} A$$
$$F = -\frac{3-4\nu}{8(1-\nu)} r_o^2 A. \tag{AII.7}$$

The final condition is obtained by imposing equilibrium of any disk of radius r. In other words, at a radial distance r, the resultant of the normal and shear stresses acting along the perimeter of the circle of radius r must be in equilibrium with the force P applied to the perimeter of the tunnel. Along the direction of the force P (horizontal direction, as shown in Fig. 4a), the resultant from the normal and shear stresses, dF, per unit length of perimeter is:

$$\mathrm{d}F = (\sigma_r \cos\theta - \tau \sin\theta) r \, d\theta. \tag{AII.8}$$

Equilibrium requires:

$$F = \int_{-\pi}^{\pi} (\sigma_r \cos\theta - \tau \sin\theta) r \, d\theta = P. \tag{AII.9}$$

This results, considering Eq. (AII.7), in:

$$A = \frac{P}{\pi} \tag{AII.10}$$

Thus, the Airy stress function for a concentrated load in plane strain in an elastic infinite medium is:

$$\phi = \frac{P}{\pi}\left[\psi r \sin\theta + \frac{1}{2} r_o \ln r - \frac{1}{2} r\theta \sin\theta - \frac{1-2\nu}{4(1-\nu)} r \ln r \cos\theta - \frac{3-4\nu}{8(1-\nu)} \frac{r_o^2}{r} \cos\theta\right]. \tag{AII.11}$$

Author's address: Dr. Antonio Bobet, Purdue University, School of Civil Engineering, 1284 Civil Engineering Building, IN 47907-1284 West Lafayette, U.S.A.; e-mail: bobet@purdue.edu